Article

Molecular Cell

HokB Monomerization and Membrane Repolarization Control Persister Awakening

Graphical Abstract

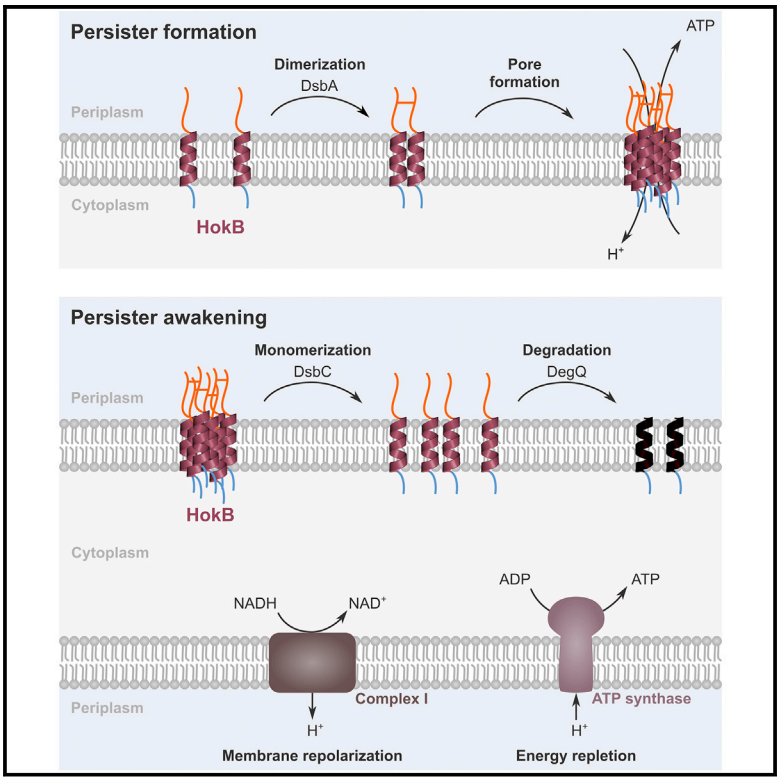

Highlights

- Dimerization of the persistence-inducing HokB toxin is essential for pore formation
- The periplasmic protease DegQ degrades HokB peptides
- HokB-persister awakening relies on HokB monomerization and membrane repolarization

Authors

Dorien Wilmaerts, Liselot Dewachter, Pieter-Jan De Loose, Celien Bollen, Natalie Verstraeten, Jan Michiels

Correspondence

jan.michiels@kuleuven.vib.be

In Brief

Wilmaerts et al. demonstrate that the toxin HokB forms intermolecular disulfide bridges, which are essential for HokB pore formation and consequently the induction of persistence. In addition, they show that the awakening of these persister cells relies on the monomerization of the HokB toxin, combined with repolarization of the membrane.

Wilmaerts et al., 2019, Molecular Cell *75*, 1031–1042
September 5, 2019
https://doi.org/10.1016/j.molcel.2019.06.015

CellPress

Molecular Cell
Article

HokB Monomerization and Membrane Repolarization Control Persister Awakening

Dorien Wilmaerts,[1,2] Liselot Dewachter,[1,2] Pieter-Jan De Loose,[1,2] Celien Bollen,[1,2] Natalie Verstraeten,[1,2,3] and Jan Michiels[1,2,3,4,*]
[1]Center for Microbiology, VIB, 3001 Leuven, Belgium
[2]Centre of Microbial and Plant Genetics, KU Leuven, 3001 Leuven, Belgium
[3]Senior authors
[4]Lead Contact
*Correspondence: jan.michiels@kuleuven.vib.be
https://doi.org/10.1016/j.molcel.2019.06.015

SUMMARY

Every bacterial population harbors a small subpopulation of so-called persisters that are transiently antibiotic tolerant. These persisters are associated with the recalcitrance of chronic infections because they can recolonize the host after antibiotic removal. Although several effectors have been described to induce persistence, persister cell awakening is poorly understood. We previously reported that the toxin HokB induces persistence via pore formation, resulting in membrane depolarization and ATP leakage. We now delineate mechanisms responsible for the awakening of HokB-induced persisters. We show that HokB dimerization by the oxidoreductase DsbA is essential for pore formation and peptide stability. Pores are disassembled via DsbC-mediated monomerization, which targets HokB for DegQ-mediated degradation. Finally, pore disassembly allows membrane repolarization by the electron transport chain, supporting cells to resume growth. These results provide a detailed view of both the formation and awakening of HokB-induced persister cells.

INTRODUCTION

Bacterial populations harbor a small fraction of persister cells that display transient tolerance to antibiotics (Michiels et al., 2016). These persisters are genetically indistinguishable from sensitive cells within the population and survive antibiotic treatment as a result of phenotypic bistability. Persisters are generally assumed to be in a slow-growing or dormant state, resulting in the inactivity of the antibiotic target (Balaban et al., 2004; Shah et al., 2006). However, the complexity of the persister phenotype likely exceeds target inactivity (Wilmaerts et al., 2019). It was shown that dormancy alone does not evoke the persistence phenotype per se (Orman and Brynildsen, 2013), and stationary phase persisters were found to be metabolically active (Orman and Brynildsen, 2015; Wilmaerts et al., 2018). In addition, persisters can be damaged by the applied antibiotic (Völzing and Brynildsen, 2015; Mok and Brynildsen, 2018), indicating that the antibiotic target is active. This heterogeneity of the persister population complicates persistence research (Michiels et al., 2016).

Toxin-antitoxin (TA) modules are associated with the formation of persister cells. Overexpression of numerous toxins increases the number of persister cells (Dörr et al., 2010; Kim and Wood, 2010; Verstraeten et al., 2015; Cheverton et al., 2016), and the deletion of toxin-encoding genes has been reported to decrease persistence in a select number of cases (Dörr et al., 2010; Wang and Wood, 2011). TA modules are plasmid-encoded or genomic elements. In general, plasmid-encoded TA modules play a role in post-segregational killing, while genomic TA modules promote survival in stressful environments and take part in mediating persistence (Page and Peti, 2016). TA modules have been classified in 6 groups based on the mechanism of toxin inhibition of the antitoxin (Page and Peti, 2016). While the toxin is typically a protein, the antitoxin can be an RNA molecule (types I and III) or a small protein (types II, IV, V, and VI).

To date, type I, type II, and type V TA modules have been implicated in persistence. In type I TA modules, the antitoxin binds with the toxin mRNA, preventing translation or triggering degradation. For type II TA modules, the protein antitoxin inhibits the protein toxin via direct binding (Harms et al., 2018). The role of type II TA modules in the formation of persister cells is under debate (Harms et al., 2017; Goormaghtigh et al., 2018; Holden and Errington, 2018). In type V TA modules, the antitoxin is an RNase that specifically degrades the toxin mRNA (Harms et al., 2018). Toxins inhibit an essential cellular function and are believed to induce persistence when their cellular concentration reaches a certain threshold value (Rotem et al., 2010). This is achieved via stress-induced upregulation of the whole TA operon, combined with stress-induced degradation of the intrinsically unstable antitoxins or by upregulation of the toxins alone (Keren et al., 2004; Muthuramalingam et al., 2016; Shan et al., 2017). In addition, both processes are suggested to happen stochastically (Rotem et al., 2010), although this hypothesis is not supported by experimental evidence.

While the induction of persistence by toxins is a well-studied phenomenon, the awakening of toxin-induced persister cells remains puzzling. One awakening strategy has been reported for *Salmonella* persisters induced by the type II toxin TacT. In this

specific case, persisters resume growth after expression of the Pth protein (Cheverton et al., 2016). In general, persister cells are believed to revert from the antibiotic-tolerant state stochastically, although environmental conditions are suggested to contribute to persister cell awakening (Dworkin and Shah, 2010; Jõers et al., 2010; Buerger et al., 2012). Upon exit from the persister state, a new population can be formed when antibiotics are removed from the environment (Michiels et al., 2016).

In previous work, we have shown that the conserved and essential guanosine triphosphatase (GTPase) ObgE induces persistence in *Escherichia coli*, thereby increasing expression of the type I toxin HokB (Verstraeten et al., 2015). HokB is a small membrane peptide that induces persistence through pore formation, thus leaking ATP and depolarizing the membrane (Verstraeten et al., 2015; Wilmaerts et al., 2018). The HokB antitoxin *sokB* is an RNA molecule that triggers the degradation of *hokB* mRNA upon binding (Gerdes, 2016). It has been hypothesized that upon membrane depolarization, the enzymatic activity of RNase E is reduced. This stabilizes *sokB* mRNA and prevents further HokB synthesis (Gerdes, 2016). Although this mechanism may explain why the HokB toxin does not evoke cell death, it does not affect the concentration of HokB peptides already present in the membrane, and, as a consequence, it cannot trigger the awakening of HokB-induced persister cells. In general, the mechanisms by which HokB-induced persisters are able to wake up remain enigmatic.

In this study, we identify mechanisms that control HokB pore formation and therefore affect both persister state entry and exit. We show that the intermolecular dimerization of HokB peptides via their periplasmic cysteine residues is effectuated by the oxidoreductase DsbA and is essential for peptide stability and pore formation. Furthermore, we demonstrate that the dormancy duration of HokB-induced persister cells is positively correlated with the concentration of HokB peptides. Awakening of HokB-induced persister cells relies on 2 essential processes. First, the HokB pore is destabilized via peptide monomerization through the periplasmic oxidoreductase DsbC. Subsequently, monomeric HokB is degraded by the DegQ protease. Second, HokB-induced persisters rely on membrane repolarization by complex I of the electron transport chain (ETC) to replenish the energy pool and allow regrowth. This work provides detailed insights into both the induction of persistence and the awakening of persister cells, which may prove useful for the development of anti-persister strategies.

RESULTS

HokB Dimerization by the Periplasmic Oxidoreductase DsbA Is Essential for Pore Formation

In previous work, we have demonstrated that the pore-forming capacity of HokB is essential for persistence and that membrane depolarization and ATP leakage are hallmarks of HokB pore formation (Verstraeten et al., 2015; Wilmaerts et al., 2018). We wanted to gain mechanistic insight about the formation of HokB pores. As the amino acid sequence of HokB contains 3 cysteine residues, we hypothesized that these residues would affect HokB pore formation by forming intermolecular disulfide bridges.

The formation of disulfide bridges between $\geq$2 HokB peptides was assessed using a non-reducing western blot. This analysis shows that HokB forms both monomers and dimers (Figure 1A). The HokB peptide contains cysteine residues at positions C9, C14, and C46. Computational predictions show that C9 and C14 are localized in the membrane, while C46 is localized in the periplasm (Wilmaerts et al., 2018). The potential contribution of these residues to dimerization was determined using HokB cysteine-to-serine substitution mutants ($HokB_{C9S}$, $HokB_{C14S}$, and $HokB_{C46S}$). First, membrane localization of the mutant peptides was confirmed (Figure S1A). Second, monomer fractions were quantified (Figure 1B). $HokB_{C46S}$ does not form dimers, demonstrating that the cysteine in the periplasm is responsible for HokB dimerization by disulfide bridge formation. Lastly, peptide concentrations were determined, showing that the concentration of $HokB_{C46S}$ is lower compared to that of HokB, possibly indicating that the absence of dimerization destabilizes the HokB peptide (Figure 1C).

A persistence assay was performed to assess whether dimerization affects HokB-mediated persistence (Figure 1D). Furthermore, in the strains expressing the cysteine-to-serine mutant peptides, we measured the membrane potential using $DiBAC_4(3)$, a stain that enters cells with a depolarized membrane (Figure S1B), and ATP leakage (Figure 1E). Both $HokB_{C9S}$ and $HokB_{C14S}$ induce persistence, depolarize the membrane, and result in ATP leakage. Conversely, $HokB_{C46S}$ does not display these phenotypes, demonstrating that it does not form pores. These results indicate that lack of pore formation results from the absence of dimerization.

Spontaneous disulfide bond formation in the periplasm of *E. coli* proceeds slowly, and free thiol groups are vulnerable to detrimental oxidation (Bardwell et al., 1991). Therefore, disulfide bond formation is performed by the periplasmic oxidoreductase DsbA (Depuydt et al., 2011). We assessed whether the dimerization of HokB is mediated by DsbA. No HokB peptides were detected in a strain lacking DsbA, indicating that HokB is unstable in a Δ*dsbA* mutant. Accordingly, HokB does not induce persistence in this mutant (Figure 1F). These data show that the absence of dimerization destabilizes HokB peptides, thereby restraining pore formation and thus the induction of persistence. Using the reducing agent dithiothreitol (DTT), we chemically mimicked the effect of the absence of *dsbA*. As expected, upon the addition of DTT, we could observe a decrease in HokB-induced persister cells (Figure S1C). In conclusion, HokB dimerization via the periplasmic C46 residue by DsbA is essential for HokB peptide stability and thus for the induction of persistence through pore formation.

Dormancy Duration Is Positively Correlated with HokB Levels

The previous experiments demonstrate that peptide stability is controlled by DsbA-mediated dimerization via periplasmic C46 residues, which is important for the induction of persistence. To assess whether HokB stability also affects persister cell awakening, we first searched for a potential correlation between the concentration of HokB peptides and awakening of HokB-induced persister cells using 2 different techniques. It has been challenging in persistence research to directly correlate the

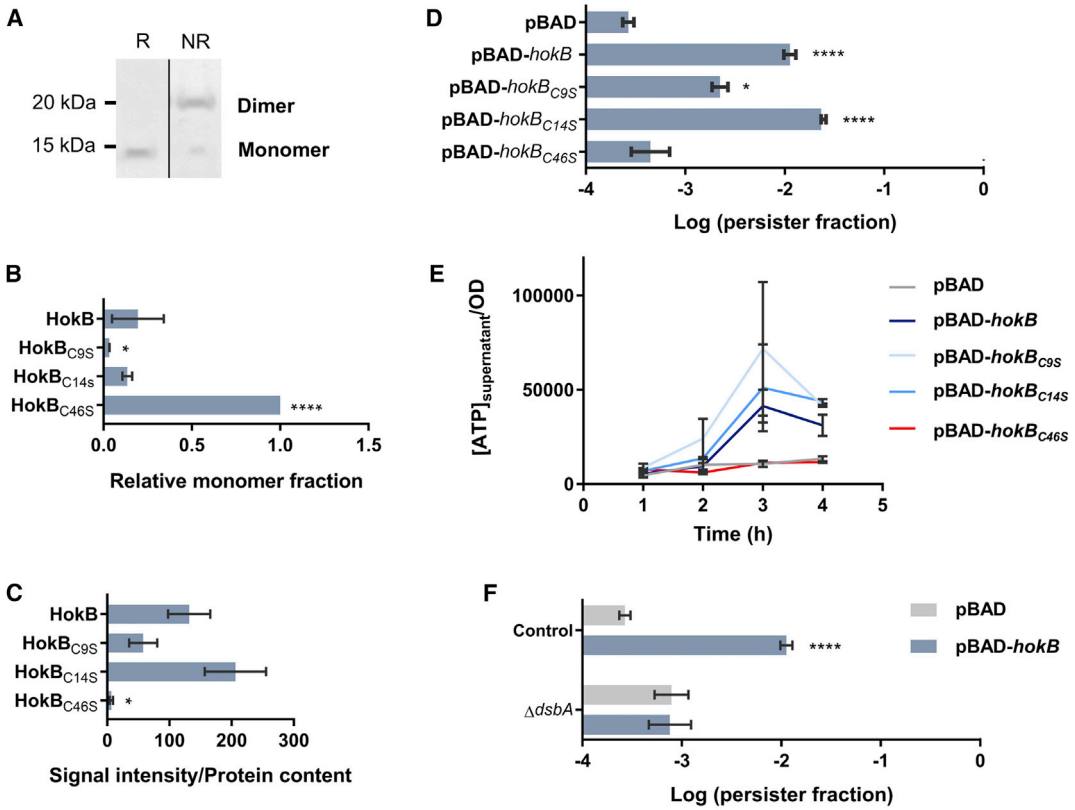

Figure 1. DsbA Forms HokB Dimers via the C46 Residue

(A) HokB peptides form dimers that can be visualized on a non-reducing (NR) western blot. Disulfide bridges are broken in a reduced sample (R). Two lanes of the same western blot are shown.

(B) A non-reducing western blot was used to quantify monomer fractions, showing that HokB$_{C46S}$ does not form dimers. The values are means ± SEMs from at least 3 independent experiments. The asterisks indicate statistical significance compared to HokB (*$p < 0.05$, ****$p < 0.0001$).

(C) A reducing western blot was performed to assess HokB peptide concentration. Signal intensities from the band were divided by the total protein concentration of the sample. HokB$_{C46S}$ is unstable compared to HokB. The values are means ± SEMs from at least 2 independent experiments. The asterisks indicate statistical significance compared to HokB (*$p < 0.05$).

(D) Expression of *hokB*$_{C46S}$ does not increase the persister fraction, in contrast to *hokB*$_{C9S}$ and *hokB*$_{C14S}$. The values are means ± SEMs from at least 3 independent experiments. The asterisks indicate statistical significance compared to the empty vector control (*$p < 0.05$, ****$p < 0.0001$). See also Figures S1A and S1B.

(E) Expression of *hokB*, *hokB*$_{C9S}$, and *hokB*$_{C14S}$ results in ATP leakage, while expression of *hokB*$_{C46S}$ does not. Values are means ± SEMs from at least 3 independent experiments. There is a significant difference ($p < 0.05$) compared to the empty vector control for time point 3 h for HokB$_{C9S}$, HokB$_{C14S}$, and HokB. After 4 h of induction, there is a significant difference compared to the empty vector control for HokB$_{C9S}$ ($p < 0.0001$), HokB$_{C14S}$ ($p < 0.0001$), and HokB ($p < 0.05$).

(F) Expression of *hokB* in a Δ*dsbA* mutant does not induce persistence. The values are means ± SEMs from at least 3 independent experiments. The asterisks indicate statistical significance compared to the empty vector control (****$p < 0.0001$). See also Figure S1C.

activity of an effector with persister awakening. Here, we took advantage of the fact that HokB is a direct effector of persistence and that its presence can be monitored using a functional mCherry-HokB fusion that effectively induces persistence (Wilmaerts et al., 2018). Furthermore, we were able to measure 73 persisters at the single-cell level, providing increased statistical power compared to previously conducted studies (Balaban et al., 2004; Goormaghtigh et al., 2018).

In a first approach, persister cells were loaded in a microfluidic device to record the time to the first cell division. The HokB peptide concentration was measured using the fluorescence intensity of mCherry-HokB. Persister cells were isolated by treating an exponentially growing culture with ceftazidime, lysing the sensitive cells but leaving the persister cells unharmed (Orman and Brynildsen, 2013). Our results show that the time to the first cell division is correlated significantly with the fluorescence intensity ($p = 0.0485$, $r = 0.4252$) (Figure 2A). The time to the first cell division varies strongly between individual persister cells, ranging from 66 to 275 min, and is normally distributed. These results were confirmed with stationary-phase cells treated with ofloxacin. Similar to the previous experiment, the time to the first cell division correlates with the fluorescence intensity ($p = 0.064$, $r = 0.4015$) (Figure 2B). Although not statistically significant, the same trend emerges, hinting at a correlation between HokB peptide concentration and dormancy duration also in the stationary phase. The time to the first cell division is normally distributed and slightly shifted upward compared to exponential-phase persisters, ranging from 112.3 to 386.2 min. The normality of the

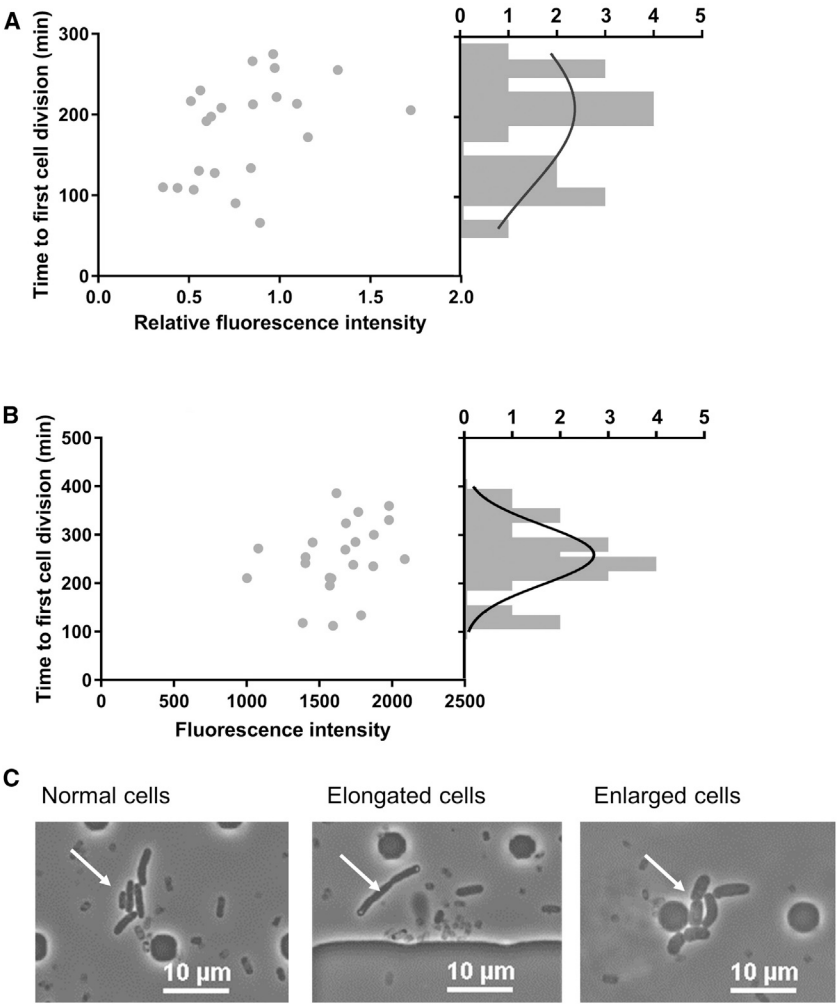

Figure 2. Monitoring Persister Outgrowth Using Microfluidics

(A) Persisters were isolated by treating an exponentially growing culture with ceftazidime. Upon persister awakening, there is a significant correlation ($p = 0.0485$, $r = 0.4252$) between the number of mCherry-HokB peptides and the time to the first cell division. Spearman correlation was used to assess statistical dependence between the 2 variables. Normality of the distribution of the time to the first cell division was assessed using the Shapiro-Wilk test. A Gauss curve is plotted on the data, giving an average time-to-first cell division of 209.8 ± 101.0 min (mean ± SD). The time to the first cell division varies from 66.1 to 275.0 min. See also Figure S2.

(B) A stationary-phase culture was treated with ofloxacin. Upon persister awakening, there is a correlation ($p = 0.064$, $r = 0.4015$) between the number of mCherry-HokB peptides and the time to the first cell division. Spearman correlation was used to assess the statistical dependence between the 2 variables. Normality of the distribution of the time to the first cell division was assessed using the Shapiro-Wilk test. A Gauss curve is plotted on the data, giving an average time-to-first cell division of 258.7 ± 61.2 min (mean ± SD). The time to first cell division varies from 112.3 to 386.2 min.

(C) Regrowing persister cells have various outgrowth phenotypes. Representative examples are shown.

distributions indicates that the awakening of HokB-induced persister cells is not a purely stochastically determined process, but it has an intrinsic time dependence, suggesting that 1 or several intermediate steps are necessary for the awakening of HokB persisters (Norman et al., 2015).

The microfluidic device allows the visualization of HokB-induced persister cells during awakening. After ceftazidime treatment, 22 persisters were visualized. In addition to 3 cells with a normal morphology, we observed 8 elongated cells and 11 enlarged cells, both giving rise to normal-size progeny (Figure 2C). These phenotypes likely result from the antibiotic treatment needed to isolate persister cells, as ceftazidime targets primarily penicillin binding protein 3 (Hayes and Orr, 1983), and loss of this protein results in elongated cells (Takeuchi et al., 2005). Ceftazidime also targets other penicillin binding proteins (1 and 2), which presumably results in the enlarged phenotype (Hayes and Orr, 1983; Sauvage et al., 2008). Following ofloxacin treatment, persisters initially regrew normally. However, in 50% of the observed events, persisters gave rise to enlarged cells after a few cell divisions. This phenotype was not inheritable, as their progeny was of a normal size. These phenotypes may indicate that many of the persister cells we observed were damaged by the applied antibiotic.

In a second approach, HokB-induced persister cells surviving ceftazidime treatment were sorted in a honeycomb plate using fluorescence activated cell sorting (FACS). The plates, containing a maximum of 1 persister cell per well, were incubated in a Bioscreen device that monitors growth by optical density measurement. Fluorescence intensity was measured during sorting. A significant correlation was observed between the lag time of growth resumption and fluorescence intensity ($p = 0.0253$, $r = 0.4148$) (Figure S2), corroborating the results of the microfluidics assays.

From these 3 experiments, we conclude that the dormancy duration of HokB-induced persister cells is positively correlated with the concentration of HokB peptides. Thus, stability of the HokB peptides may be of importance, not only for the induction of HokB persister cells but also for their awakening. Therefore, we hypothesized that proteases may be targeting HokB and reduce its stability, thereby contributing to the awakening process.

HokB Is a Substrate of the Protease DegQ

To identify HokB-degrading proteases, we quantified HokB peptide levels following the overexpression of different *E. coli* proteases using the ASKA library (Kitagawa et al., 2005). We selected 5 periplasmic proteases based on their putative function or target (DegP, DegQ, MepA, PtrA, Prc), and as a control 2

proteases localized in the inner membrane (RseP, FtsH) and 3 cytoplasmic proteases (ElaD, HslU, HslV). Expression of *degQ, ftsH*, and *prc* reduces the concentration of HokB peptides (Figure S3A); however, only overexpression of *degQ* abolishes HokB-induced membrane depolarization (Figure S3B). Therefore, further experiments focused on the periplasmic serine protease DegQ. DegQ targets β-branched side chains lacking disulfide bonds (Kolmar et al., 1996; Waller and Sauer, 1996), which is in accordance with computational predictions indicating that the periplasmic part of HokB contains 2 β strands (Bar-Yaacov et al., 2017) and with our observation that HokB monomers are unstable. Using a newly constructed plasmid that encodes the native DegQ protein, without the His_6-tag present in the ASKA library, we confirmed that the overexpression of *degQ* reduces the concentration of HokB peptides by 82% ($p = 0.00002$) (Figure 3A) and abolishes HokB-induced membrane depolarization (Figure 3B). Furthermore, the overexpression of *degQ* results in the abolishment of HokB-induced persistence (Figure 3C). The latter observation is in agreement with a decreased ATP leakage in a strain that co-expresses both *degQ* and *hokB* for 4 h (Figure 3D).

To further confirm the role of DegQ, the effect of *degQ* deletion on HokB stability was examined. These experiments show that the concentration of HokB peptides is 2-fold higher in a Δ*degQ* mutant compared to the wild-type background (Figure 3E). However, expression of *hokB* in a Δ*degQ* mutant depolarizes the membrane to the same extent as in the control strain (Figure 3F). Our data show that the periplasmic DegQ protease controls the HokB peptide concentration. Deletion of *degQ* reduces the level of HokB-induced persisters 3-fold (Figure 3G). This is surprising, given the higher stability of the peptides and the same number of cells with a depolarized membrane, which would suggest that the number of persisters would be equal. As absence of persister awakening also results in a decreased persister fraction, our data suggest that degradation of HokB by DegQ may play a role in the awakening of HokB-induced persister cells. As DegQ only degrades β sheets devoid of a disulfide bridge (Kolmar et al., 1996; Waller and Sauer, 1996), we hypothesized that DegQ would not be the only factor at play.

HokB Degradation Requires Peptide Monomerization by the Oxidoreductase DsbC

So far, we have established that HokB peptides are stabilized by DsbA-mediated dimerization, and our data suggest that persister awakening relies on the degradation of HokB by DegQ. While monomeric HokB peptides are detected in *E. coli* (Figures 1A and 1B), the oxidative state of the periplasm impedes the reduction of disulfide bonds at a frequent rate, which is a requirement for DegQ to degrade proteins (Kolmar et al., 1996; Waller and Sauer, 1996). An interesting candidate to assist in DegQ-mediated degradation of HokB is DsbC. This oxidoreductase uses electrons originating from nicotinamide adenine dinucleotide phosphate (NADPH) and passed along by the thioredoxin TrxA to reduce disulfide bonds generated by DsbA (Depuydt et al., 2011). We reasoned that DsbC could monomerize HokB peptides. Corroborating this hypothesis, we could not detect any HokB monomers in a strain lacking DsbC (Figure 4A). Next, we assessed whether monomerization by DsbC is essential for the DegQ-mediated degradation of HokB peptides. For this, HokB and DegQ were co-expressed in a Δ*dsbC* mutant, and the concentration of HokB peptides was measured quantitatively (Figure 4B). As shown before, DegQ significantly reduces HokB peptide levels by >80% in a wild-type strain. However, in the absence of DsbC, expression of *degQ* does not significantly reduce HokB levels. This indicates that the monomerization of HokB by DsbC is important for the DegQ-mediated degradation of HokB.

To assess whether persister levels are altered in a Δ*dsbC* mutant, a persistence assay was performed in this mutant. As expected, HokB does not increase the persister fraction. However, the expression of *hokB* has a dominant-negative effect in the absence of DsbC as it significantly decreases the persister fraction in comparison to a vector control (Figure 4C). This effect is abolished by the addition of the disulfide-reducing compound DTT, indicating that it results from disulfide bridge formation (Figure S4A). We next sought to identify the origin of this dominant-negative effect. Although HokB possesses only a single cysteine residue exposed in the periplasm (C46), it was shown that the tyrosine at position 29 is affected by an adenosine-to-inosine RNA editing system, occasionally resulting in an additional periplasmic cysteine at position 29 (Bar-Yaacov et al., 2017). We reasoned that DsbC may break disulfide bonds between C29 and C46 of a single HokB peptide and that this reduction is essential for persistence. To verify this, we performed a persistence assay following the expression of $hokB_{Y29}$, which contains a non-editable tyrosine codon at position 29 (Figure 4C; Bar-Yaacov et al., 2017). In a wild-type background, $hokB_{Y29}$ expression still increases persistence, indicating that RNA editing does not affect HokB-mediated persistence. However, the presence of a non-editable tyrosine at position 29 abolishes the dominant-negative effect of HokB expression in the Δ*dsbC* mutant. As DsbA preferentially forms a disulfide bridge between 2 consecutive cysteine residues (Depuydt et al., 2011), the dominant-negative effect therefore likely results from the absence of isomerization of HokB after RNA editing, resulting in cell death after 2 to 3 cell divisions (Figure S4B). This is in line with a previous report showing that genetically substituting Y29 by a cysteine induces cell death (Bar-Yaacov et al., 2017).

The absence of high persister counts following *hokB* expression in Δ*dsbC* mutants can be explained either by an impaired induction of persistence or an impaired awakening of persister cells. As we have previously discovered a link between pore functioning and persistence (Wilmaerts et al., 2018), we hypothesized that in the case of impaired induction of persistence, HokB pores would not be functional. Therefore, different characteristics of HokB pore functioning (i.e., membrane depolarization and ATP leakage) (Verstraeten et al., 2015; Wilmaerts et al., 2018) were assessed in the Δ*dsbC* mutant. $HokB_{Y29}$ was used instead of HokB in the Δ*dsbC* mutant to avoid incorrect ATP measurements resulting from cell lysis. As is the case in the wild-type, expression of $hokB_{Y29}$ in a Δ*dsbC* mutant still evokes membrane depolarization (Figure 4D) and ATP leakage (Figure 4E), indicating that HokB still forms functional pores in the absence of DsbC. These findings suggest that all of the mechanisms are in place to induce persistence and that the low persister level upon *hokB* expression in a Δ*dsbC* strain is due to an impaired awakening of persister cells.

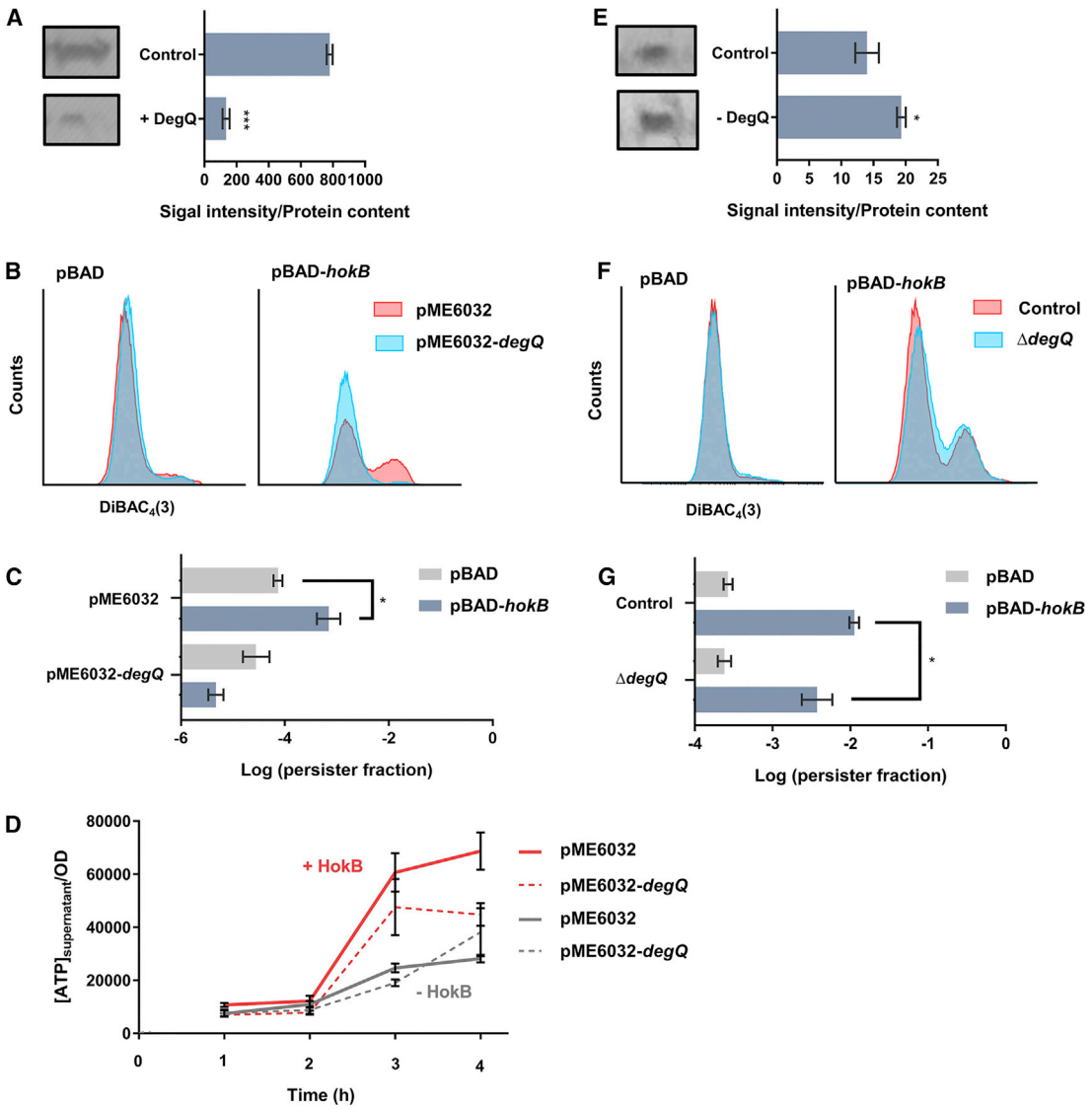

Figure 3. HokB Is a Substrate of the Periplasmic Protease DegQ

(A) A reducing western blot was performed to assess the HokB peptide concentration. Signal intensities from the band were divided by the total protein concentration of the sample. Expression of *degQ* decreases the concentration of HokB peptides in the population by 82.75% ± 0.02% (mean ± SEM). A representative example of 3 biological repeats is depicted. The values are means ± SEMs from at least 3 independent experiments. The asterisks indicate statistical significance (***$p < 0.0001$). The images shown were obtained from a single western blot. See also Figure S3A.

(B) The membrane potential was measured using $DiBAC_4(3)$, showing that HokB does not induce membrane depolarization upon co-expression with *degQ*. A representative example of 3 biological repeats is depicted. See also Figure S3B.

(C) Overexpression of *degQ* abolishes HokB-mediated persistence. The values are means ± SEMs from at least 3 independent experiments. The asterisks indicate statistical significance (*$p < 0.05$).

(D) Expression of *degQ* results in a decreased concentration of ATP in the supernatant after 4 h of induction of both *degQ* and *hokB*. Values are means ± SEMs from at least 3 independent experiments. $p < 0.05$ for the comparison of pBAD and pBAD-*hokB* for both pME6032 and pME6032-*degQ* after 3 h of induction; $p < 0.05$ for the comparison of pBAD and pBAD-*hokB* for pME6032 after 4 h of induction.

(E) A reducing western blot was performed to assess the HokB peptide concentration. Signal intensities from the band were divided by the total protein concentration of the sample. HokB peptides are stabilized in a *degQ* deletion mutant. A representative example of 3 biological repeats is depicted. The values are means ± SEMs from at least 3 independent experiments. The asterisks indicate statistical significance (*$p < 0.05$). The images shown were obtained from a single western blot.

(F) Expression of *hokB* in a *degQ* deletion mutant does not statistically affect the number of cells with a depolarized membrane. A representative example of 3 biological repeats is shown.

(G) *degQ* deletion significantly decreases HokB-mediated persistence. The values are means ± SEMs from at least 3 independent experiments. The asterisks indicate statistical significance (*$p < 0.05$).

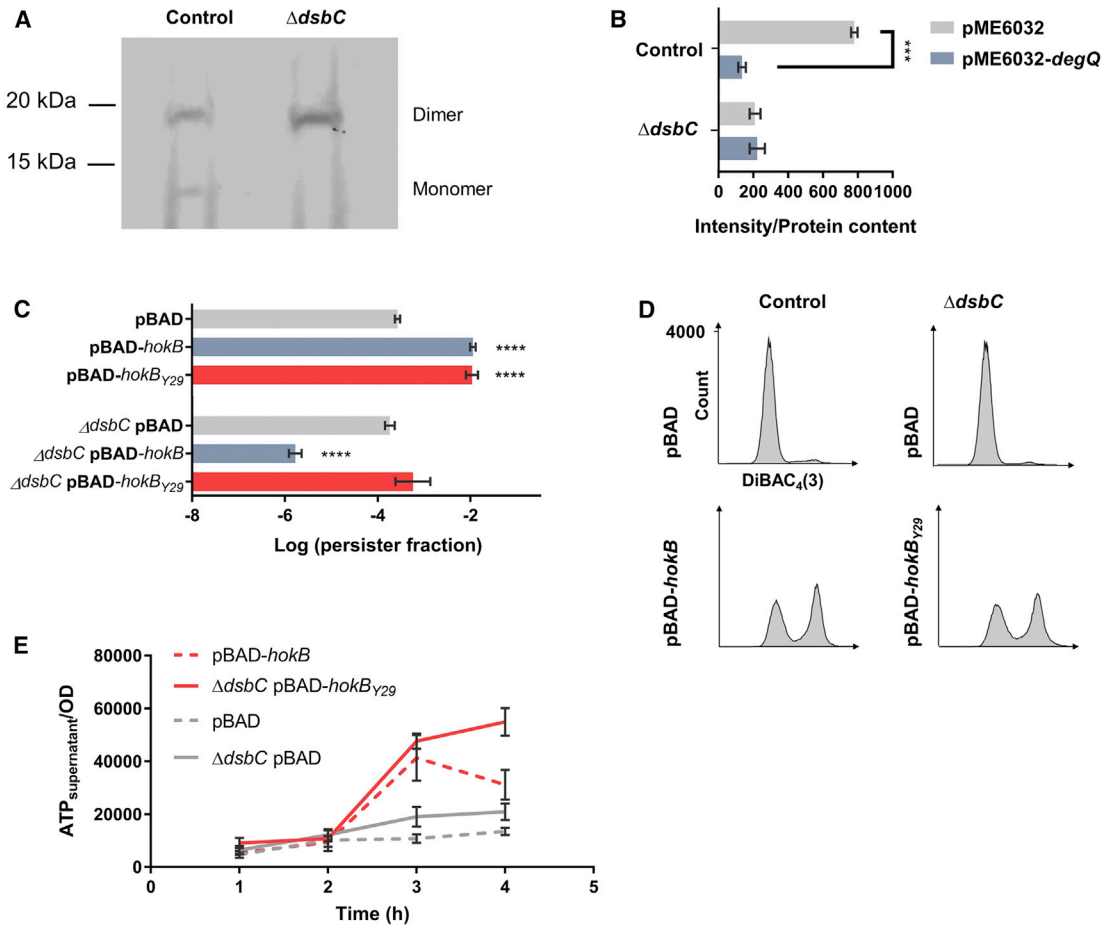

Figure 4. HokB Pores Are Functional in a Δ*dsbC* Mutant

(A) In the absence of DsbC, 100% of HokB peptides are in the dimer form. A representative example of 3 independent experiments is shown.

(B) A reducing western blot was performed to assess the HokB peptide concentration. Signal intensities from the band were divided by the total protein concentration of the sample. DegQ-mediated degradation of HokB is constrained in a ΔΔ*dsbC* mutant. HokB peptide levels upon *degQ* expression are diminished significantly in the wild-type background, in contrast to the Δ*dsbC* mutant. The values are means ± SEMs from at least 3 independent experiments. The asterisks indicate statistically significant differences from the vector control (***$p < 0.0001$). Data for the wild-type background are identical to the data shown in Figure 3A.

(C) Expression of *hokB* in a Δ*dsbC* mutant causes a dominant negative effect, which results from RNA editing, as expression of *hokB*$_{Y29}$ does not cause this phenotype. The expression of *hokB*$_{Y29}$ in the wild type does not affect persistence. The values are means ± SEMs from at least 3 independent experiments. The asterisks indicate statistically significant differences from the empty vector control (****$p < 0.0001$). See also Figures S4A and S4B.

(D) Expression of *hokB* depolarizes the membrane in the wild-type background and in a Δ*dsbC* mutant. A representative example of at least 3 independent repeats is shown.

(E) HokB pores result in ATP leakage after 3 h of induction in both the wild-type mutant and the Δ*dsbC* mutant. The values are means ± SEMs from at least 3 independent experiments. After 3 h of induction, $p < 0.05$ for the comparison of pBAD and pBAD-*hokB* in both backgrounds.

Absence of the Complex I Component NuoA Impairs Persister Awakening

Reduction of the disulfide bridge between HokB peptides renders these peptides vulnerable to DegQ-mediated degradation, resulting in pore disassembly. We have previously shown that HokB induces membrane depolarization and ATP leakage (Wilmaerts et al., 2018). Therefore, we hypothesized that in addition to pore disassembly, persister awakening also requires repolarization of the membrane to replenish cellular ATP levels.

To assess whether repolarization of the membrane is required for persister awakening, we used a mutant deprived of *nuoA*. NuoA is part of the NADH-dehydrogenase complex I (NDH-I), which consists of 13 subunits encoded by the *nuo* operon. Deletion of 1 gene in the operon abolishes complex I activity (Erhardt et al., 2012). NDH-I translocates 2 protons to the periplasm per transported electron, and as a consequence, disruption affects the ability of the cell to repolarize the membrane. As expected, the effect of *hokB* expression on persistence is severely reduced in a Δ*nuoA* mutant (Figure 5A). HokB pores are functional in the Δ*nuoA* mutant, as there is still membrane depolarization and ATP leakage (Figures 5B and 5C). These data are similar to the results obtained for the Δ*dsbC* mutant and indicate that persister awakening is impaired in the absence of NuoA.

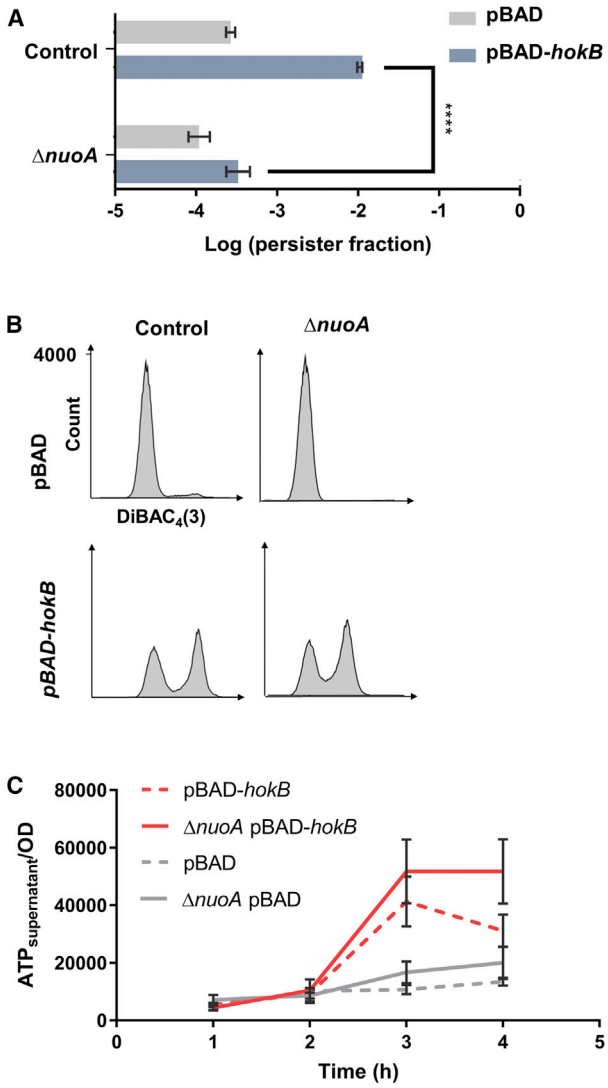

Figure 5. HokB Pores Are Functional in a Δ*nuoA* Mutant

(A) HokB-mediated persistence is strongly impaired in a Δ*nuoA* mutant. The values are means ± SEMs from at least 3 independent experiments. The asterisks indicate statistically significant differences (****$p < 0.0001$).

(B) Membrane depolarization upon *hokB* expression was assessed using $DiBAC_4(3)$, showing that HokB still collapses the membrane potential in the Δ*nuoA* mutant. A representative example of 3 independent experiments is shown.

(C) HokB pores result in ATP leakage after 3 h of induction in both the wild-type mutant and the Δ*nuoA* mutant. The values are means ± SEMs from at least 3 independent experiments. After 3 h of induction, $p < 0.05$ for the comparison of pBAD and pBAD-*hokB* in both backgrounds.

Awakening of HokB-Induced Persisters Relies on Peptide Monomerization and Membrane Repolarization

The preceding experiments demonstrate that HokB pores are functional in the Δ*dsbC* and Δ*nuoA* mutants (Figures 4D, 4E, 5B, and 5C), even though persister counts are not increased in these mutants following *hokB* expression (Figures 4C and 5A). This suggests that the awakening of HokB-induced persisters is impeded. To validate this hypothesis, the lag phase of individual persisters was assessed in various deletion mutants. In a wild-type background, HokB-induced persisters have a shortened lag phase compared to the empty vector control (Wilmaerts et al., 2018). However, expression of $hokB_{Y29}$ in Δ*dsbC* and *hokB* in Δ*nuoA* mutants delays awakening (Figure 6A), indicating that regrowth is impaired. To confirm that DsbC-mediated monomerization is important for awakening, we assessed the lag phase following *hokB* expression in a Δ*trxA* mutant that has an impaired electron transport toward DsbC (Depuydt et al., 2011). The

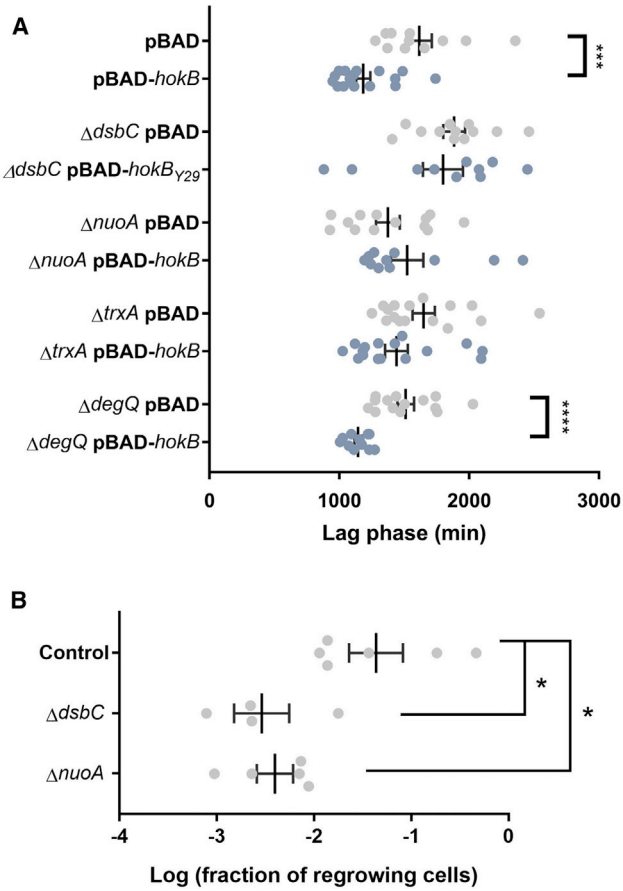

Figure 6. Awakening of HokB-Induced Persister Cells Is Hindered in the Absence of Monomerization and Membrane Repolarization

(A) HokB-induced persister cells have a shortened lag phase in the wild-type mutant and in the Δ*degQ* mutant. This reduction in lag phase is not observed when expressing $hokB_{Y29}$ in Δ*dsbC* and *hokB* in Δ*trxA* and Δ*nuoA* mutants. The values are means ± SEMs from at least 3 independent experiments. The asterisks indicate statistically significant differences from the empty vector control (***$p < 0.001$, ****$p < 0.0001$).

(B) Stationary-phase cultures expressing *hokB* ($hokB_{Y29}$ in the case of the Δ*dsbC* mutant) were treated with antibiotics and stained with redox sensor green (RSG). The latter emits green fluorescence when cells are metabolically active and therefore acts as a measure for reducing capacity. For each sample, 10,000 highly fluorescent cells were sorted and plated. The number of colonies after antibiotic treatment was divided by the number of colonies of the control sample, after which the log was taken. Data from at least 3 independent experiments are represented and indicate the fraction of viable cells that are able to grow in the population after antibiotic treatment. Values represent mean ± SEM from three independent experiments. The asterisks indicate statistically significant differences from the empty vector control (*$p < 0.05$).

abolishment of the reducing capacity of DsbC delays the regrowth of HokB-induced persister cells (Figure 6A), corroborating the importance of disulfide bridge reduction for awakening. Deletion of *degQ* does not affect the lag phase of HokB-induced persister cells, indicating that disassembly of HokB pores but not degradation of the constituting peptides drives persister awakening (Figure 6A).

Our data show that the absence of DsbC and NuoA delays HokB-induced persister cell awakening (Figure 6A). However, this does not explain the decreased persister fraction in these mutants compared to the wild type expressing *hokB* (Figures 4C and 5A). When quantifying persisters by plate counting, a mere delay in awakening would eventually yield similar persister counts. Therefore, we hypothesized that the absence of HokB monomerization or membrane repolarization restrains the growth resumption of HokB-induced persister cells and, hence, colony formation. To demonstrate that the population has more viable cells than is assessed through plate counting, 10,000 metabolically active cells were sorted and the number of colonies on plate was counted. The data presented in Figure 6B show that the fraction of regrowing cells is significantly higher in the wild-type control compared to the Δ*dsbC* and Δ*nuoA* mutants. This demonstrates that HokB-induced persister cells display reduced awakening in the absence of DsbC-mediated monomerization or complex I-mediated membrane repolarization.

DISCUSSION

Several toxins have been implicated in persistence, but a detailed mode of action remains unknown in many cases (Korch and Hill, 2006; Dörr et al., 2010; Tripathi et al., 2014). In previous work, we have shown that the conserved GTPase ObgE induces *hokB*, a type I toxin that is widespread among Gram-negative bacteria (Verstraeten et al., 2015). Furthermore, we have demonstrated that HokB forms pores that result in ATP leakage, which is linked with the induction of persistence (Wilmaerts et al., 2018). In the present study, we have identified several factors affecting HokB peptide stability, and we have demonstrated that this stability plays a crucial role in both the induction of persistence and the awakening process of HokB-induced persister cells.

DsbA-Mediated Dimerization of HokB Is Required to Induce Persistence

In a wild-type background, the majority of the HokB peptides is detected in its dimeric form, with a relative monomer fraction of ~20%. Our results support a model in which dimerization is effectuated by the periplasmic oxidoreductase DsbA and results in an intermolecular disulfide bridge between 2 periplasmic cysteine residues at position C46. The lower concentration of $HokB_{C46S}$ and the observation that HokB cannot be detected in a Δ*dsbA* mutant demonstrate that HokB monomers are unstable. This accords with earlier observations, demonstrating that disulfide bridge formation stabilizes a peptide (Denoncin and Collet, 2013). In addition, the expression of $HokB_{C46S}$ does not increase persister levels, indicating that dimerization is required for the induction of persistence. A tyrosine-to-cysteine change at position 29 mediated by RNA editing presumably results in DsbA preferentially forming an intramolecular disulfide bridge between the 2 consecutive C29 and C46 residues (Depuydt et al., 2011). This intramolecular bridge was shown to be deleterious to the cell (Bar-Yaacov et al., 2017), and our data are indicative of a rescue mechanism that is mediated by the disulfide oxidoreductase DsbC.

HokB Peptide Destabilization and Membrane Repolarization Modulate Persister Awakening

Tracking regrowth via microfluidics and single-cell sorting revealed a positive correlation between the dormancy duration of HokB-induced persister cells and the concentration of HokB peptides. This is in line with previous research conducted using an exponentially growing *E. coli* population, for which it was shown that the duration of growth arrest depends on the concentration of the HipA toxin (Rotem et al., 2010). Regrowing HokB-induced persister cells have aberrant outgrowth phenotypes, which likely result from the antibiotic treatment. This demonstrates that the antibiotic target in persister cells is active, confirming an earlier report on persister cells acquiring DNA damage following antibiotic treatment (Völzing and Brynildsen, 2015).

The normal distribution of the time to first cell division of HokB-induced persister cells indicates that 1 or multiple intermediate steps activate the awakening process (Norman et al., 2015). In addition, the positive correlation between the concentration of HokB peptides and the dormancy duration in persister cells suggests that molecular mechanisms initialize awakening by destabilizing HokB peptides, eventually resulting in pore disassembly. We found that HokB peptide destabilization is controlled by the oxidoreductase DsbC. In the absence of DsbC, HokB peptides are exclusively in the dimer configuration and form functional pores, as there is membrane depolarization and ATP leakage. However, the expression of *hokB* in a Δ*dsbC* mutant does not increase persister counts, suggesting that awakening is impaired in this mutant. Corroborating this finding, the fraction of cells that are metabolically active but unable to grow is higher in a Δ*dsbC* mutant compared to the wild type. Some persisters do wake up, however, at a rate that is comparable to the empty vector control. The origin of these persisters can either be HokB independent or HokB dependent. In the latter case, the disulfide bridge may be reduced by other reducing compounds in the periplasm, such as glutathione (Ke and Berkmen, 2014).

HokB-induced persister cells display ATP leakage and membrane depolarization (Verstraeten et al., 2015; Wilmaerts et al., 2018). We reasoned that to resume growth, DsbC-mediated pore disassembly should be followed by the replenishment of cellular energy pools and the repolarization of the membrane. We found that membrane repolarization by complex I of the ETC plays a major role in HokB-persister cell awakening, although the role of the other units of the ETC cannot be excluded. The absence of complex I leaves HokB pore characteristics unaltered. However, the number of metabolically active cells that are unable to grow is increased in a mutant deprived of complex I, and regrowth of persister cells is delayed. In conclusion, peptide destabilization by DsbC-mediated monomerization as well as repolarization of the membrane are essential for awakening of HokB-induced persister cells.

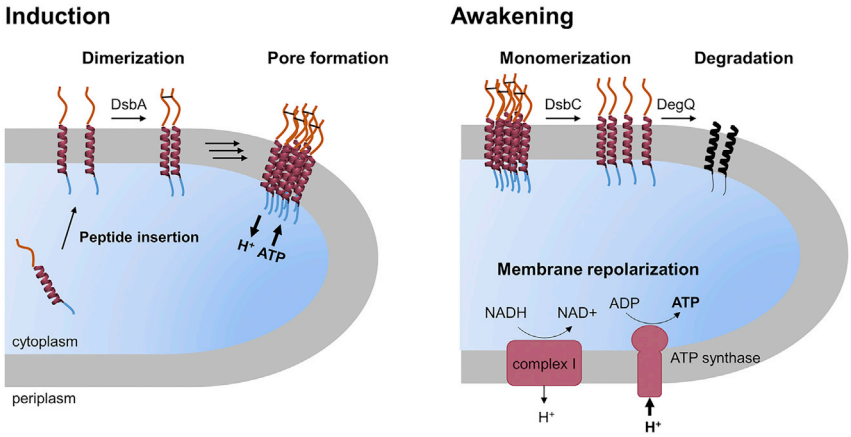

Figure 7. Model of HokB-Mediated Persister Induction and Awakening

Upon HokB peptide insertion in the membrane, DsbA catalyzes the formation of a disulfide bridge between the C46 residues of 2 HokB monomers. This stabilizes HokB peptides, allowing pore formation. Pore formation results in the leakage of protons and ATP out of the cell, inducing persistence. HokB pores are destabilized via DsbC-mediated monomerization. This targets HokB peptides for degradation by DegQ. Once the pore is dysfunctional, the electron transport chain is able to repolarize the membrane and replenish the ATP pool, eventually resulting in persister cell awakening. Of note, an intramolecular bridge between a C29 residue and the C46 residue can be formed after adenosine-to-inosine RNA editing of tyrosine 29. However, this bridge is not implicated in the persister phenotype.

DegQ Degrades HokB Monomers

Following monomerization by DsbC, the HokB peptides need to be degraded to prevent re-dimerization and thus re-formation of the pore. Our results show that HokB peptide levels are controlled by the periplasmic DegQ protease. To the best of our knowledge, this is the first report of a protease targeting a type I toxin. DegQ is known to cleave next to an isoleucine or a valine residue (Kolmar et al., 1996), the latter of which is present in the periplasmic amino acid sequence of HokB at position 40. Cleaving off the V40 residue would remove the C46 residue, thereby preventing re-dimerization of HokB peptides by DsbA. DegQ shows the highest activity at a relatively low pH of 5.5 *in vitro* (Sawa et al., 2011). The average periplasmic pH of *E. coli* is 7.5 (Wilks and Slonczewski, 2007), and although it is unlikely that membrane repolarization would result in a periplasmic pH of 5.5, a small decrease due to proton translocation may modulate the awakening of HokB-induced persister cells by triggering DegQ-mediated degradation.

Although the deletion of *degQ* affects HokB-induced persistence to a certain extent, the awakening of HokB-induced persister cells is not delayed in a Δ*degQ* mutant. This is in contrast to our results with Δ*dsbC* and Δ*nuoA* mutants, and it may indicate that peptide destabilization and repolarization are the primary factors modulating awakening or that the delayed lag phase in Δ*dsbC* and Δ*nuoA* mutants is HokB independent. Alternatively, other proteases may take over upon *degQ* deletion, which is plausible given their redundant character (Sklar et al., 2007).

A Model for Induction and Awakening of HokB-Induced Persister Cells

Here, we propose a model that explains both the induction and awakening of HokB-induced persister cells (Figure 7). Following HokB peptide insertion into the membrane, the periplasmic oxidoreductase DsbA forms an intermolecular disulfide bridge, thereby stabilizing HokB peptides and allowing pore formation. The latter causes ATP leakage and membrane depolarization, ultimately inducing persistence. Upon awakening, the oxidoreductase DsbC reduces the disulfide bridge, which disassembles the pore and allows the ETC to repolarize the membrane and produce ATP. Repolarization lowers the pH, which in turn activates DegQ to cleave off a part of the periplasmic domain of HokB monomers, thereby preventing re-dimerization. This ultimately results in the regrowth of HokB-induced persister cells.

STAR★METHODS

Detailed methods are provided in the online version of this paper and include the following:

- KEY RESOURCES TABLE
- LEAD CONTACT AND MATERIALS AVAILABILITY
- EXPERIMENTAL MODEL AND SUBJECT DETAILS
- METHOD DETAILS
  - Bacterial Strain Construction
  - Persistence Assay
  - Purification of the Membrane Fraction and Western Blot
  - Measuring the Membrane Potential
  - Measuring ATP in the Supernatant
  - Measuring the Time to First Cell Division Using Microfluidics
  - Measuring Single-Cell Lag Time
  - Measuring the Lag Time after Fluorescence Activated Cell Sorting
  - Assessing Viable Cells in the Population
- QUANTIFICATION AND STATISTICAL ANALYSIS
  - Persistence Assay
  - Measuring ATP Leakage and Single-Cell Lag Times and Determining Viable Cells
  - Determination of Relative Monomer Fraction and Total Protein Concentration
  - Correlation Analysis
  - Determination of Statistical Difference Between Flow Cytometric Data
- DATA AND CODE AVAILABILITY

SUPPLEMENTAL INFORMATION

Supplemental Information can be found online at https://doi.org/10.1016/j.molcel.2019.06.015.

ACKNOWLEDGMENTS

This work was supported by grants from the Fonds Wetenschappelijk Onderzoek (FWO) (G055517N, G047112N, and G0B2515N), the Interuniversity Attraction Poles-Belgian Science Policy Office IAP-BELSPO (IAP P7/28), KU Leuven (C16/17/006), and the Flanders Institute for Biotechnology (VIB). We thank Serge Beullens for the technical assistance with FACS and David De Coster for assistance with western blotting.

AUTHOR CONTRIBUTIONS

D.W. designed and performed the experiments, analyzed the data, and wrote the manuscript. L.D., N.V., and J.M. designed the experiments, discussed the results, and edited the manuscript. P.-J.D.L. and C.B. assisted in performing the experiments.

DECLARATION OF INTERESTS

The authors declare no competing interests.

Received: February 13, 2019
Revised: May 21, 2019
Accepted: June 12, 2019
Published: July 18, 2019

REFERENCES

Baba, T., Ara, T., Hasegawa, M., Takai, Y., Okumura, Y., Baba, M., Datsenko, K.A., Tomita, M., Wanner, B.L., and Mori, H. (2006). Construction of *Escherichia coli* K-12 in-frame, single-gene knockout mutants: the Keio collection. Mol. Syst. Biol. *2*, 0008.

Balaban, N.Q., Merrin, J., Chait, R., Kowalik, L., and Leibler, S. (2004). Bacterial persistence as a phenotypic switch. Science *305*, 1622–1625.

Bar-Yaacov, D., Mordret, E., Towers, R., Biniashvili, T., Soyris, C., Schwartz, S., Dahan, O., and Pilpel, Y. (2017). RNA editing in bacteria recodes multiple proteins and regulates an evolutionarily conserved toxin-antitoxin system. Genome Res. *27*, 1696–1703.

Bardwell, J.C., McGovern, K., and Beckwith, J. (1991). Identification of a protein required for disulfide bond formation in vivo. Cell *67*, 581–589.

Buerger, S., Spoering, A., Gavrish, E., Leslin, C., Ling, L., and Epstein, S.S. (2012). Microbial scout hypothesis, stochastic exit from dormancy, and the nature of slow growers. Appl. Environ. Microbiol. *78*, 3221–3228.

Cheverton, A.M., Gollan, B., Przydacz, M., Wong, C.T., Mylona, A., Hare, S.A., and Helaine, S. (2016). A *Salmonella* toxin promotes persister formation through acetylation of tRNA. Mol. Cell *63*, 86–96.

Datsenko, K.A., and Wanner, B.L. (2000). One-step inactivation of chromosomal genes in *Escherichia coli* K-12 using PCR products. Proc. Natl. Acad. Sci. USA *97*, 6640–6645.

Denoncin, K., and Collet, J.F. (2013). Disulfide bond formation in the bacterial periplasm: major achievements and challenges ahead. Antioxid. Redox Signal. *19*, 63–71.

Depuydt, M., Messens, J., and Collet, J.F. (2011). How proteins form disulfide bonds. Antioxid. Redox Signal. *15*, 49–66.

Dörr, T., Vulić, M., and Lewis, K. (2010). Ciprofloxacin causes persister formation by inducing the TisB toxin in *Escherichia coli*. PLoS Biol. *8*, e1000317.

Dworkin, J., and Shah, I.M. (2010). Exit from dormancy in microbial organisms. Nat. Rev. Microbiol. *8*, 890–896.

Erhardt, H., Steimle, S., Muders, V., Pohl, T., Walter, J., and Friedrich, T. (2012). Disruption of individual nuo-genes leads to the formation of partially assembled NADH:ubiquinone oxidoreductase (complex I) in *Escherichia coli*. Biochim. Biophys. Acta *1817*, 863–871.

Francois, K., Devlieghere, F., Standaert, A.R., Geeraerd, A.H., Van Impe, J.F., and Debevere, J. (2003). Modelling the individual cell lag phase. Isolating single cells: protocol development. Lett. Appl. Microbiol. *37*, 26–30.

Gerdes, K. (2016). 'Hypothesis: type I toxin-antitoxin genes enter the persistence field-a feedback mechanism explaining membrane homoeostasis. Philos. Trans. R. Soc. Lond. B Biol. Sci. *371*, 20160189.

Goormaghtigh, F., Fraikin, N., Putrinš, M., Hallaert, T., Hauryliuk, V., Garcia-Pino, A., Sjödin, A., Kasvandik, S., Udekwu, K., Tenson, T., et al. (2018). Reassessing the role of type II toxin-antitoxin systems in formation of *Escherichia coli* type II persister cells. MBio *9*, e00640-e18.

Harms, A., Fino, C., Sørensen, M.A., Semsey, S., and Gerdes, K. (2017). Prophages and growth dynamics confound experimental results with antibiotic-tolerant persister cells. MBio *8*, e01964-e17, https://doi.org/10.1128/mBio.01964-17.

Harms, A., Brodersen, D.E., Mitarai, N., and Gerdes, K. (2018). Toxins, targets, and triggers: an overview of toxin-antitoxin biology. Mol. Cell *70*, 768–784.

Hayes, M.V., and Orr, D.C. (1983). Mode of action of ceftazidime: affinity for the penicillin-binding proteins of *Escherichia coli* K12, *Pseudomonas aeruginosa* and *Staphylococcus aureus*. J. Antimicrob. Chemother. *12*, 119–126.

Holden, D.W., and Errington, J. (2018). Type II toxin-antitoxin systems and persister cells. MBio *9*, e10574-e18.

Jõers, A., Kaldalu, N., and Tenson, T. (2010). The frequency of persisters in *Escherichia coli* reflects the kinetics of awakening from dormancy. J. Bacteriol. *192*, 3379–3384.

Ke, N., and Berkmen, M. (2014). Production of disulfide-bonded proteins in *Escherichia coli*. Curr. Protoc. Mol. Biol. *108*, 1–21.

Keren, I., Shah, D., Spoering, A., Kaldalu, N., and Lewis, K. (2004). Specialized persister cells and the mechanism of multidrug tolerance in *Escherichia coli*. J. Bacteriol. *186*, 8172–8180.

Kim, Y., and Wood, T.K. (2010). Toxins Hha and CspD and small RNA regulator Hfq are involved in persister cell formation through MqsR in *Escherichia coli*. Biochem. Biophys. Res. Commun. *391*, 209–213.

Kitagawa, M., Ara, T., Arifuzzaman, M., Ioka-Nakamichi, T., Inamoto, E., Toyonaga, H., and Mori, H. (2005). Complete set of ORF clones of *Escherichia coli* ASKA library (a complete set of *E. coli* K-12 ORF archive): unique resources for biological research. DNA Res. *12*, 291–299.

Kolmar, H., Waller, P.R.H., and Sauer, R.T. (1996). The DegP and DegQ periplasmic endoproteases of *Escherichia coli*: specificity for cleavage sites and substrate conformation. J. Bacteriol. *178*, 5925–5929.

Korch, S.B., and Hill, T.M. (2006). Ectopic overexpression of wild-type and mutant *hipA* genes in *Escherichia coli*: effects on macromolecular synthesis and persister formation. J. Bacteriol. *188*, 3826–3836.

Michiels, J.E., Van den Bergh, B., Verstraeten, N., and Michiels, J. (2016). Molecular mechanisms and clinical implications of bacterial persistence. Drug Resist. Updat. *29*, 76–89.

Mok, W.W.K., and Brynildsen, M.P. (2018). Timing of DNA damage responses impacts persistence to fluoroquinolones. Proc. Natl. Acad. Sci. USA *115*, E6301–E6309.

Muthuramalingam, M., White, J.C., and Bourne, C.R. (2016). Toxin-antitoxin modules are pliable switches activated by multiple protease pathways. Toxins (Basel) *8*, 214–230.

Norman, T.M., Lord, N.D., Paulsson, J., and Losick, R. (2015). Stochastic switching of cell fate in microbes. Annu. Rev. Microbiol. *69*, 381–403.

Orman, M.A., and Brynildsen, M.P. (2013). Dormancy is not necessary or sufficient for bacterial persistence. Antimicrob. Agents Chemother. *57*, 3230–3239.

Orman, M.A., and Brynildsen, M.P. (2015). Inhibition of stationary phase respiration impairs persister formation in E. coli. Nat. Commun. *6*, 7983.

Page, R., and Peti, W. (2016). Toxin-antitoxin systems in bacterial growth arrest and persistence. Nat. Chem. Biol. *12*, 208–214.

Rotem, E., Loinger, A., Ronin, I., Levin-Reisman, I., Gabay, C., Shoresh, N., Biham, O., and Balaban, N.Q. (2010). Regulation of phenotypic variability by a threshold-based mechanism underlies bacterial persistence. Proc. Natl. Acad. Sci. USA *107*, 12541–12546.

Sauvage, E., Kerff, F., Terrak, M., Ayala, J.A., and Charlier, P. (2008). The penicillin-binding proteins: structure and role in peptidoglycan biosynthesis. FEMS Microbiol. Rev. *32*, 234–258.

Sawa, J., Malet, H., Krojer, T., Canellas, F., Ehrmann, M., and Clausen, T. (2011). Molecular adaptation of the DegQ protease to exert protein quality control in the bacterial cell envelope. J. Biol. Chem. *286*, 30680–30690.

Shah, D., Zhang, Z., Khodursky, A., Kaldalu, N., Kurg, K., and Lewis, K. (2006). Persisters: a distinct physiological state of *E. coli*. BMC Microbiol. *6*, 53.

Shan, Y., Brown Gandt, A., Rowe, S.E., Deisinger, J.P., Conlon, B.P., and Lewis, K. (2017). ATP-dependent persister formation in Escherichia coli. MBio *8*, e02267-e16.

Shaner, N.C., Campbell, R.E., Steinbach, P.A., Giepmans, B.N., Palmer, A.E., and Tsien, R.Y. (2004). Improved monomeric red, orange and yellow fluorescent proteins derived from *Discosoma* sp. red fluorescent protein. Nat. Biotechnol. *22*, 1567–1572.

Sklar, J.G., Wu, T., Kahne, D., and Silhavy, T.J. (2007). Defining the roles of the periplasmic chaperones SurA, Skp, and DegP in *Escherichia coli*. Genes Dev. *21*, 2473–2484.

Takeuchi, S., DiLuzio, W.R., Weibel, D.B., and Whitesides, G.M. (2005). Controlling the shape of filamentous cells of *Escherichia coli*. Nano Lett. *5*, 1819–1823.

Tripathi, A., Dewan, P.C., Siddique, S.A., and Varadarajan, R. (2014). MazF-induced growth inhibition and persister generation in *Escherichia coli*. J. Biol. Chem. *289*, 4191–4205.

Verstraeten, N., Knapen, W.J., Kint, C.I., Liebens, V., Van den Bergh, B., Dewachter, L., Michiels, J.E., Fu, Q., David, C.C., Fierro, A.C., et al. (2015). Obg and membrane depolarization are part of a microbial bet-hedging strategy that leads to antibiotic tolerance. Mol. Cell *59*, 9–21.

Völzing, K.G., and Brynildsen, M.P. (2015). Stationary-phase persisters to ofloxacin sustain DNA damage and require repair systems only during recovery. MBio *6*, e00731.

Waller, P.R.H., and Sauer, R.T. (1996). Characterization of *degQ* and *degS, Escherichia coli* genes encoding homologs of the DegP protease. J. Bacteriol. *178*, 1146–1153.

Wang, X., and Wood, T.K. (2011). Toxin-antitoxin systems influence biofilm and persister cell formation and the general stress response. Appl. Environ. Microbiol. *77*, 5577–5583.

Wilks, J.C., and Slonczewski, J.L. (2007). pH of the cytoplasm and periplasm of *Escherichia coli*: rapid measurement by green fluorescent protein fluorimetry. J. Bacteriol. *189*, 5601–5607.

Wilmaerts, D., Bayoumi, M., Dewachter, L., Knapen, W., Mika, J.T., Hofkens, J., Dedecker, P., Maglia, G., Verstraeten, N., and Michiels, J. (2018). The persistence-inducing toxin HokB forms dynamic pores that cause ATP leakage. MBio *9*, e00744-e18.

Wilmaerts, D., Windels, E.M., Verstraeten, N., and Michiels, J. (2019). General mechanisms leading to persister formation and awakening. Trends Genet. *35*, 401–411.

Zwietering, M.H., Jongenburger, I., Rombouts, F.M., and van 't Riet, K. (1990). Modeling of the bacterial growth curve. Appl. Environ. Microbiol. *56*, 1875–1881.

STAR★METHODS

KEY RESOURCES TABLE

REAGENT or RESOURCE	SOURCE	IDENTIFIER
Antibodies		
anti-His6 (mouse IgG1) monoclonal antibodies	Sigma-Aldrich	AB_840258
HisProbe™-HRP	Thermo Scientific™	Cat#15165
anti-Mouse IgG – Alkaline Phosphatase	Sigma-Aldrich	AB_1839782
Bacterial and Virus Strains		
TOP10	Invitrogen™	Cat#C404003
K-12 Keio collection	NBRP	N/A
Deposited Data		
Western blots and Coomassie stainings	This paper	https://doi.org/10.17632/gr3thzhmhp.2
Original data for persistence assays, ATP leakage measurements, western blots, single-cell lag phases, flow cytometric analysis and correlation assays	This paper	https://doi.org/10.17632/gr3thzhmhp.2
Oligonucleotides		
Forward *dsbA:* AGAACCCCCTTTGCAATTAA	IDT	N/A
Reverse *dsbA:* GCAACAATAACACCTGTAGC	IDT	N/A
Forward *dsbC:* ATCACCGACCACAATAATCC	IDT	N/A
Reverse *dsbC:* GTTTACTGGCTGGAAACCTA	IDT	N/A
Forward *nuoA:* ACGTTCTTTGCCGATAGATT	IDT	N/A
Reverse *nuoA*: GCAGAACGTACAAAACTGTT	IDT	N/A
Forward *degQ:* TACCATGGCGCACGACTATC	IDT	N/A
Reverse *degQ:* CTGCATCATGACCGCTAGCC	IDT	N/A
Forward *trxA:* AGGGCGAAGTCGGAAAACTT	IDT	N/A
Reverse *trxA:* CATGTCTTTTCGCTGCCTGG	IDT	N/A
Recombinant DNA		
$HokB_{C9S}$: CACCCTCGAGATGAAGCACAACCCTCTGGTGGTGTCCCTGC TCATTATCTGCATTACGATTCTGACATTCACACTCCTGACC CGACAAACGCTCTACGAACTGCGGTTCCGGGACGGTGATA AGGAGGTTGCTGCGCTCATGGCCTGCACGTCCAGGTAAGG GCAAGCGCGGGGATTTTCCCCGCGCATTTGACTAGCAGATT CATTTTCTCATGGCACCCCTTTTACACTTCAGTTAGTGCATG TTTTTTTCGATGCACTAATAGAACCATCATTACAGACAAAT TTGCCGCCTGCCGTACAGTGTGAGATCCCAAGCTTGATC	IDT	N/A
$HokB_{C14S:}$ CACCCTCGAGATGAAGCACAACCCTCTGGTGGTGTGTCTGC TCATTATCTCCATTACGATTCTGACATTCACACTCCTGACC CGACAAACGCTCTACGAACTGCGGTTCCGGGACGGTGATA AGGAGGTTGCTGCGCTCATGGCCTGCACGTCCAGGTAAGG GCAAGCGCGGGGATTTTCCCCGCGCATTTGACTAGCAGATT CATTTTCTCATGGCACCCCTTTTACACTTCAGTTAGTGCATG TTTTTTTCGATGCACTAATAGAACCATCATTACAGACAAAT TTGCCGCCTGCCGTACAGTGTGAGATCCCAAGCTTGATC	IDT	N/A
$HokB_{C46S:}$ CACCCTCGAGATGAAGCACAACCCTCTGGTGGTGTGTCTGC TCATTATCTGCATTACGATTCTGACATTCACACTCCTGACC CGACAAACGCTCTACGAACTGCGGTTCCGGGACGGTGATA AGGAGGTTGCTGCGCTCATGGCCTCCACGTCCAGGTAAGG GCAAGCGCGGGGATTTTCCCCGCGCATTTGACTAGCAGATT CATTTTCTCATGGCACCCCTTTTACACTTCAGTTAGTGCATG TTTTTTTCGATGCACTAATAGAACCATCATTACAGACAAAT TTGCCGCCTGCCGTACAGTGTGAGATCCCAAGCTTGATC	IDT	N/A

(*Continued on next page*)

Continued

REAGENT or RESOURCE	SOURCE	IDENTIFIER
Software and Algorithms		
FlowJo	BD	SCR_008520 https://www.flowjo.com/solutions/flowjo/downloads

LEAD CONTACT AND MATERIALS AVAILABILITY

Further information and requests for recourses and reagents should be directed to and will be fulfilled by the Lead Contact, Jan Michiels (jan.michiels@kuleuven.vib.be).

EXPERIMENTAL MODEL AND SUBJECT DETAILS

E. coli TOP10, obtained from Invitrogen (USA), was used in all experiments. Bacteria were grown in autoclaved lysogeny broth (LB) at 37°C. Liquid cultures were incubated with orbital shaking (200 rpm) in the presence of appropriate antibiotics. Strains containing the pBAD/His A plasmid were cultured in LB with 100 μg ml^{-1} ampicillin. Strains containing the pME6032 plasmid were cultured in LB with 10 μg ml^{-1} tetracycline.

METHOD DETAILS

Bacterial Strain Construction

The Δ*dsbA*, Δ*dsbC,* Δ*nuoA,* Δ*degQ* and Δ*trxA* knockout mutants were made by homologous recombination following the protocol of Datsenko and Wanner (2000). PCR products were generated from the Keio collection (Baba et al., 2006). The following primers were used to amplify a kanamycin resistance cassette flanked by FLP recombinase target sites: AGAACCCCCTTTGCAATTAA and GCAA CAATAACACCTGTAGC (Δ*dsbA*), ATCACCGACCACAATAATCC and GTTTACTGGCTGGAAACCTA (Δ*dsbC*), ACGTTCTTTGCCGA TAGATT and GCAGAACGTACAAAACTGTT (Δ*nuoA*), TACCATGGCGCACGACTATC and CTGCATCATGACCGCTAGCC (Δ*degQ*) and AGGGCGAAGTCGGAAAACTT and CATGTCTTTTCGCTGCCTGG (Δ*trxA*). Electrocompetent cells were generated by diluting an overnight culture of TOP10 containing the plasmid PKD46, encoding for a phage lambda Red recombinase, 100-fold and incubating the strain at 30° for 2 h. Thereafter, arabinose (0.2%) was added and the culture was again incubated for 2h at 30°. 1 mL culture was centrifuged and washed four times with ice-cold milliQ water. The obtained PCR product was introduced in electrocompetent cells and inserted in the genome by the phage lambda Red recombinase. After electroporation, cells were plated out on plates containing 40 μg mL^{-1} kanamycin. Insertion of the kanamycin cassette was assessed by determining the size of the PCR product of the site of interest.

For the construction of pBAD/His A-*hokB*$_{C9S}$, pBAD/His A-*hokB*$_{C14S}$ and pBAD/His A-*hokB*$_{C46S}$, gene blocks (Table S1) were ordered from IDT (USA) and cloned in pBAD/His A using KpnI and HindIII restriction. The mutated *hokB* fragments were amplified by PCR using primers CACCGGTACCGGATCAGGTTCCGGCTCTAAGCACAACCCTCTGG and ATCGAAGCTTTTACCTGGACGTGCA. The PCR products were digested with KpnI and HindIII and cloned into pBAD/*Myc*-His A-*mCherry* (Shaner et al., 2004). Similarly, pBAD/His A-*hokB*$_{Y29}$ was constructed by amplifying the mutated *hokB*-fragment from pBAD/*Myc*-His A-*mCherry-hokB*$_{Y29}$ (Bar-Yaacov et al., 2017) and transferring the resulting product to pBAD/His A. The protease-encoding genes *degQ*, *mepA*, *hslU*, *elaD*, *rseP*, *degP*, *ptrA*, *prc*, *ftsH* and *hslV* were expressed using plasmids from the ASKA library (Kitagawa et al., 2005). pME6032-*degQ* was constructed by amplifying *degQ* from *E. coli* BW25113 using primers CACCGGTACCATGAAAAAACAAACC and ACTGCTCGAGT TAACGATCAGCAG. The PCR product was digested using KpnI and XhoI and cloned into PME6032. Construction of pBAD/*Myc*-His A-*perceval,* pBAD/His A-*hokB* and pBAD/*Myc*-His A-*mCherry-hokB* was described previously (Verstraeten et al., 2015; Wilmaerts et al., 2018).

Persistence Assay

Persistence assays were performed in stationary phase. Overnight cultures were diluted 100-fold in 250 mL flasks containing 100 mL LB medium, appropriate antibiotics (ampicillin (100 μg mL^{-1}) and/or tetracycline (10 μg mL^{-1})) and inducer (0.2% arabinose and/or IPTG (1mM)). For experiments shown in Figures S1C and S4A, DTT was prepared freshly, filter sterilized, and added at a concentration of 10 μM or 3 mM to the LB medium after autoclaving. Cultures were incubated for 16-18 h, after which 990 μL was treated with 5 μg mL^{-1} ofloxacin (10 μL sterile water was added to the control). After 5 h incubation, samples were serially diluted in 10 mM $MgSO_4$, plated on LB-agar plates and incubated for 48 h at 37°C. The number of colony forming units (CFUs) was determined by plate counting.

Purification of the Membrane Fraction and Western Blot

Overnight cultures were diluted 100-fold and induced in test tubes with 5 mL LB, and appropriate inducers and antibiotics were added. After 16 h incubation, 2 mL of culture was spun down (13000 rpm, 5 min) and frozen overnight at −20°. Samples were dissolved in 300 μL EDTA-free protease inhibitor, 100 mM iodoacetamide (IAM) and benzonase (all purchased from Sigma Aldrich). Samples were sonicated for 2 min at 15% amplitude with a Branson digital sonifier, after which they were centrifuged for 70 min at 15000 rpm at 4°C. After centrifugation, the supernatant was removed and the pellet was dissolved in 8 M urea (purchased from VWR International) and 100 mM IAM. Samples were dissolved in NuPAGE LDS Sample buffer (Invitrogen) (for a reducing western blot in combination with NuPAGE LDS Reducing agent (Invitrogen)), and incubated for 20 min at 70°C, after which they were loaded on a Novex ® 12% Tris-Glycine Gel (Invitrogen) in MES-buffer in a Novex Bolt Mini Gel tank.

Proteins were transferred using a XCell Sure Lock on a PVDF Membrane filter paper in CAPS buffer. The membrane was blocked for 1 h using bovine serum albumin (BSA) (1%) dissolved in TBS buffer, and subsequently washed with TBS in case anti-His6 (mouse IgG1) monoclonal antibodies (Sigma-Aldrich) were used at a concentration of 0.2 $\mu g\ mL^{-1}$, as recommended by the manufacturer. In case HisProbe™-HRP (Thermo Scientific™) antibodies were used, at a concentration of 1 $\mu g\ mL^{-1}$, the membrane was blocked for 2 h using skimmed milk and 0.1% Tween20. After blocking, the membrane was incubated overnight at 4°C in shaking conditions. The membrane was washed using 0.1% Tween20 in TBS buffer. In case anti-His6 monoclonal antibodies were used, anti-Mouse IgG – Alkaline Phosphatase (Sigma Aldrich) antibodies were incubated for 1 h at room temperature at a concentration of 1.2 $\mu g\ mL^{-1}$, as recommended by the manufacturer, after which the blot was washed using 0.1% Tween20 in TBS buffer. Following the color reaction, a picture was taken from the blot using a Canon EOS 1300D camera, after which the picture was reverted to grayscale using GIMP software. Using the HisProbe™-HRP, detection occurred immediately after washing using the Clarity™ Western ECL Substrate (Bio-Rad) and the Fusion FX imaging system (Vilber Lourmat).

Pictures were uploaded to Image Studio Lite®, after which signal intensities from the bands could be detected. For quantitative assays of protein concentration between different strains, corrections of the signal intensities were made based on the total protein concentration of the sample, measured using the Qubit™ protein assay kit (Invitrogen™).

Measuring the Membrane Potential

The membrane potential was measured as described before (Wilmaerts et al., 2018). Briefly, strains incubated overnight were diluted 100-fold in PBS buffer containing $DIBAC_4(3)$ (Invitrogen™).

Measuring ATP in the Supernatant

The concentration of ATP in the supernatant was measured as described before (Wilmaerts et al., 2018). Briefly, strains incubated overnight were diluted 100-fold in 100 mL LB medium, after which the cells were kept on ice for 5 min and centrifuged for 10 min at 5000 rpm. 100 μL BacTiter-Glo reagent (Promega, USA) was added to 100 μL of the supernatant. After 5 min incubation at room temperature, bioluminescence and OD (595 nm) measurements were taken for every well. The bioluminescence was divided over the OD.

Measuring the Time to First Cell Division Using Microfluidics

An overnight culture was diluted 100 times in 5 mL LB. For exponential-phase cultures, bacteria were incubated for 3 h at 37°C, after which they were treated with ceftazidime (500 $\mu g\ mL^{-1}$) for 4 h. For stationary-phase cultures, samples were incubated for 16h at 37°C, after which they were treated with ofloxacin (5 $\mu g\ mL^{-1}$) for 5 h. Following antibiotic treatment, cells were spun down at low speed (3000 rpm, 5 min) and dissolved in LB medium that was preheated to 37°C. The microfluidic device was prepared following the manufacturer's instructions. After cell loading, fluorescence images were taken immediately using a Nikon Eclipse Ti-E inverted microscope with a CFI Plan Apochromat 100X objective with a numerical aperture of 1.45. Fluorescence intensity of the cells was analyzed using the NIS Elements Analysis 4.4 software (Nikon, Japan). LB was added to the chamber with a pressure of 1.2 psi for 24 h at 37°C. Phase-contrast images were taken every 15 min for 24 h. For exponential-phase persisters, differences in fluorescence intensity of the population between different days were taken into account by calculating the average fluorescence intensity of the surviving cells (not lysed) and dividing it by the fluorescence intensity of the regrowing persister cells. For stationary-phase cells, all persisters originated from a single experiment.

Measuring Single-Cell Lag Time

Single-cell lag times were measured as described before (Wilmaerts et al., 2018). Briefly, cells were incubated an treated with antibiotics as described for the persistence assay. After ofloxacin treatment (5 $\mu g\ mL^{-1}$), cells were resuspended in LB, after which a twofold dilution series was prepared. A growth curve was obtained by incubating cells in a Bioscreen C device under continuous shaking at 37°C. If two consecutive wells displayed no growth, the well before was assigned to contain a single cell (Francois et al., 2003). Single-cell lag times were calculated using the Gompertz equation (Zwietering et al., 1990).

Measuring the Lag Time after Fluorescence Activated Cell Sorting

Antibiotic treatment was performed as described for the microfluidics assay. Subsequently, samples were dissolved in PBS buffer (pH = 7.4) at room temperature and individual cells were immediately collected in a honeycomb plate. During sorting, the

fluorescence intensity of each cell was linked with its position. Sorting was gated on the forward and side scatter of a non-treated population. After sorting, the plates were incubated in a Bioscreen C device under continuous shaking at 37°C for 48 h and the OD at 595 nm was measured every 15 min. The lag phase of each persister cell was calculated from the growth curve using the Gompertz equation (Zwietering et al., 1990). To take into account differences in fluorescence intensity of the population between different days, the average fluorescence intensity of the surviving cells was calculated and divided by the fluorescence intensity of the resuscitated persister cells.

Assessing Viable Cells in the Population

A persister assay in stationary phase was performed as described above. Antibiotic-treated cells were centrifuged (3000 rpm, 5 min) and dissolved in 1 mL PBS in combination with redox sensor green (RSG), purchased from Invitrogen (USA). For the control samples, 20 μL of the untreated culture was taken and dissolved in 1 mL PBS with RSG. After 10 min incubation at room temperature, cells were sorted based on a high RSG value, which was determined using exponentially-growing cells that had grown for 3 h after 100-fold dilution in 5 mL LB. After determining the appropriate gate, 10 000 cells were sorted in 1 mL PBS for both conditions. After sorting, the antibiotic-treated samples were centrifuged (3000 rpm, 5 min) and diluted in 110 μL 10 mM $MgSO_4$, after which they were plated on LB agar plates. The control samples were directly diluted in 10 mM $MgSO_4$, after which they were plated on LB agar plates. Plates were incubated for 48 h at 37°C and the number of CFUs was quantified by plate counting. To determine the fraction of cells that, after antibiotic treatment, was able to regrow in the whole population of viable cells, the number of CFUs per mL of the antibiotic-treated sample was divided by the number of CFUs per mL of the control sample. Cells were sorted using a BD influx cell sorter (BD Biosciences, USA) and RSG fluorescence was measured using a 488-nm laser and a 520-nm filter. Data were analyzed using FlowJo V10 (BD Biosciences, USA).

QUANTIFICATION AND STATISTICAL ANALYSIS

Persistence Assay

Statistical calculations were performed on log10-transformed data and were used to verify potential differences in persister fractions. Statistical comparisons were based on ANOVA with a Tukey's post hoc test for multiple comparisons for more than two populations, and an unpaired two-sided t test was used to compare the means of two populations.

Measuring ATP Leakage and Single-Cell Lag Times and Determining Viable Cells

Statistical comparisons were made using an unpaired two-sided t test.

Determination of Relative Monomer Fraction and Total Protein Concentration

Statistical comparisons for the relative monomer fractions for the substitution mutants were based on ANOVA with a Dunnett's post hoc test for multiple comparisons. To determine a statistical difference between total protein concentrations, corrected by the total protein concentration, unpaired two-sided t test were used to compare the means of two populations. Differences in signal intensity over the total protein content are explained by the presence of the pME6032 plasmid (Figure 3A). Additionally, the differences in signal intensities over the total protein content between the HokB controls in Figures 1C and 3E result from using different detection methods. For Figure 1C, HisProbe-HRP antibodies were used, while for Figure 3E, anti-His6 monoclonal antibodies were used.

Correlation Analysis

Spearman correlation was used to determine the correlation between time to first cell division and fluorescence intensity.

Determination of Statistical Difference Between Flow Cytometric Data

Statistical differences between flow cytometric data were assessed using the Chi squared comparison algorithm of the FlowJo software. The obtained T(x) values between *hokB* expressed in the wild-type background and the Δ*degQ* mutant were not statistically different from the controls.

DATA AND CODE AVAILABILITY

Original data for persistence assays, ATP leakage measurements, western blots, single-cell lag phases, flow cytometric analysis, and correlations assays in the paper have been published on Mendeley: https://doi.org/10.17632/gr3thzhmhp.2